THE JOURNAL OF PHYSICAL CHEMISTRY B
A JOURNAL OF THE AMERICAN CHEMICAL SOCIETY

pubs.acs.org/JPCB

Article

Structural Forces in Ionic Liquids: The Role of Ionic Size Asymmetry

J. Pedro de Souza,[⊥] Karina Pivnic,[⊥] Martin Z. Bazant, Michael Urbakh, and Alexei A. Kornyshev*

Cite This: *J. Phys. Chem. B* 2022, 126, 1242−1253

Read Online

ACCESS | Metrics & More | Article Recommendations | Supporting Information

ABSTRACT: Ionic liquids (ILs) are charged fluids composed of anions and cations of different size and shape. The ordering of charge and density in ILs confined between charged interfaces underlies numerous applications of IL electrolytes. Here, we analyze the screening behavior and the resulting structural forces of a representative IL confined between two charge-varied plates. Using both molecular dynamics simulations and a continuum theory, we contrast the screening features of a more-realistic asymmetric system and a less-realistic symmetric one. The ionic size asymmetry plays a nontrivial role in charge screening, affecting both the ionic density profiles and the disjoining pressure distance dependence. Ionic systems with size asymmetry are stronger coupled systems, and this manifests itself both in their response to the electrode polarization and spontaneous structure formation at the interface. Analytical expressions for decay lengths of the disjoining pressure are obtained in agreement with the pressure profiles computed from molecular dynamics simulations.

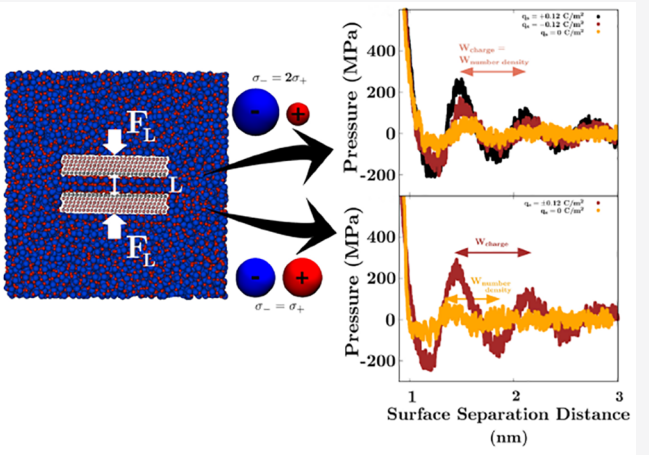

1. INTRODUCTION

Room-temperature ionic liquids (ILs) are molten salts composed of majorly asymmetrically sized anions and cations.[1,2] ILs have wide electrochemical stability windows, low vapor pressure, and are thermally stable.[3,4] Because of their exceptional properties, they are used in energy storage applications including supercapacitors and batteries[3] and as solvents for reactions and for catalysis.[2] They can also be employed as electrotunable lubricants.[5,6] In these applications, the ILs can be confined in charged nanopores down to the nanometer scale, in which the extent of the nanopore confinement and its polarity determine the interfacial IL structure and charge layering.[7−10]

To optimize the interfacial behavior of ILs for their many applications, researchers need to accurately model ILs. This is done either through computationally expensive atomistic simulations or via sophisticated theoretical approaches, which go beyond standard mean-field theories of dilute electrolyte solutions. In such highly concentrated electrolytes as ILs, the dilute solution theory is predestined to fail since ILs form structures determined by dense packing of ions in the *crowding*[11−16] (layering of ions of the same charge at highly charged electrodes) and *overscreening*[17,18] (alternating layers of opposite charge at weakly charged electrodes) regimes. Most egregiously, the dilute solution theoretical description does not take into account the ionic size.[11,19,20] To capture these screening features, multiple continuum theories have been developed to include the finite size of ions in their steric and electrostatic interactions, especially for concentrated systems at high voltages.[21−26] The simplest theoretical models of these systems have been developed for the case of ions of the same size. This was natural to do as a start, although most ILs exhibit strong size asymmetry. In theories, ion asymmetry has typically been studied within the mean field approach that accounted for crowding, particularly in the explanation of the asymmetry of the double-layer differential capacitance curves in such systems.[3,12,27−31] In molecular dynamics (MD) simulations, ion asymmetry has been either specially introduced[18] or naturally included with fully atomistic or coarse grained models of ions.[3] Certain classical Density Functional Theories (DFT) have also been applied to asymmetric ILs, predicting interfacial layering in line with MD simulations.[24,32] These studies of ILs draw from the wide body of theoretical research on primitive model electrolytes either through classical DFT[33−37] or integral equation theories.[38−43] In fact, earlier work from Greberg and Kjellander revealed the role of asymmetry in the contact behavior and decay of bulk correlations in primitive model electrolytes.[44]

Received: November 1, 2021
Revised: January 4, 2022
Published: February 8, 2022

https://doi.org/10.1021/acs.jpcb.1c09441
J. Phys. Chem. B 2022, 126, 1242−1253

Surface force apparatus (SFA) and atomic force microscopy (AFM) measurements have emerged as the main experimental tools to investigate the nanoscale structure of interfacial liquids,[45] including ILs.[7,8,46,47] While in SFA experiments the mica surfaces are spontaneously negatively charged, the AFM setup can incorporate conductive electrodes, allowing for the independent control of charges on the surfaces. Both SFA and AFM measurements have been performed in a variety of ILs, and in all cases decaying oscillatory forces were observed, with an oscillation period of the order of an ion pair diameter (usually dominated by the largest ion diameter), indicative of the underlying alternating charge layering structure.[8,9,47,48] At even longer ranges than the oscillatory forces, SFA measurements found an additional monotonically decaying "tail" of the force, both in concentrated electrolytes and ILs.[48−51]

Despite these findings, however, simulations and theoretical descriptions of primitive model electrolytes have not succeeded to recover the existence of such a tail.[34] Long-range electrostatic forces in the dilute limit can be described by analytical formulas derived from Debye−Huckel linearization, but such simple analytical equations are not readily available for the oscillatory structural forces. While the above-mentioned theories presented sophisticated analyses of the role of asymmetry on interfacial ionic behavior, they still did not present simplified, explicit formulas for the oscillatory IL structure and structural forces, nor did they directly validate the role of asymmetry on the structural forces and screening structure by MD simulations of the concentrated IL limit in varying extents of confinement. Instead of directly applying theoretically derived formulas, the experimental oscillatory forces are typically empirically fitted to an oscillatory decaying function. Therefore, the physical and quantitative interpretation of oscillatory structural forces in experiments could greatly benefit from analytical formulas derived within theories of concentrated, and generally asymmetric ILs.

In the present work, we go further into investigating the double layer structure of an asymmetric IL under confinement between equally charged surfaces using both MD simulations and an advanced continuum theory. The ion density profiles and disjoining pressure curves that we calculate based on the original theory[22] show qualitative and quantitative agreement with the results of simulations for a range of surface charge densities and surface separations. By a comparison of a representative IL with asymmetric ions to an IL composed of size-symmetric ions, we demonstrate that the size asymmetry strongly determines the ionic layering structure between two flat charged interfaces. Even at *zero charge of the electrode* there is an entropy-driven "preferential adsorption" of smaller ions, which results in *spontaneous layering of positive and negative charges near the electrode*. The order of layering may, in fact, be changed by specific adsorption of any of these ions, which is not included in our simple model, but which could easily be modeled by adding a specific term in the interaction potential between the ions and the surface. In whatever direction that effect could have shifted the result, it would act at the background of the noted effect.

Furthermore, the size asymmetry leads to a strong coupling of charge density and number density oscillations even far from the interface that is absent for the symmetric case. Analytical approximations are shown to reproduce the simulated modes of decaying oscillations in the disjoining pressure at the nanometer scale. However, neither the simulations nor the theory contain any evidence of an abnormally long decay length or long-range exponential tails. Nevertheless, the main value of the theory lies in the analytical description of the decaying modes of the structural forces and their dependence on surface charging in terms of the IL physical properties. The numerical predictions of the full nonlinear theory can be generated with much smaller computational cost compared to atomistic simulations.

All in all, the presented theory, backed up by the MD simulations, demonstrates that the ion asymmetry in electrostatic and steric interactions are essential in describing the double layer structure for ultraconcentrated, asymmetric ILs. These findings therefore signify an important step in the advancement of our understanding of the screening behavior and the resulting structural forces of ultraconcentrated, asymmetric ILs as well as of solvent-in-salt systems, under nanoconfinements.

2. SIMULATIONS AND THEORY

In this paper, an IL is approximated in both MD simulations and a continuum theory, first with asymmetric anion and cation sizes, and then with an equal anion and cation size, as charged Lennard-Jones (LJ) spheres. Such level of simplification has been chosen first of all to investigate the effects not obscured by any chemical complexity of the ions, and secondly because this would allow the most straightforward comparison between the simulations and the theory that we use here. We highlight the properties and parameters of the MD simulations and the continuum theory before applying them to model the IL and the resulting disjoining pressures. For convenience, the symbols which appear in the theory are summarized and listed in the Glossary of Symbols at the end of the article.

2.1. Simulation Details. Within this minimal model, the ions are represented as a 1:1 mixture of oppositely and singly charged LJ spheres,[18,52,53] as shown in Figure 1. The

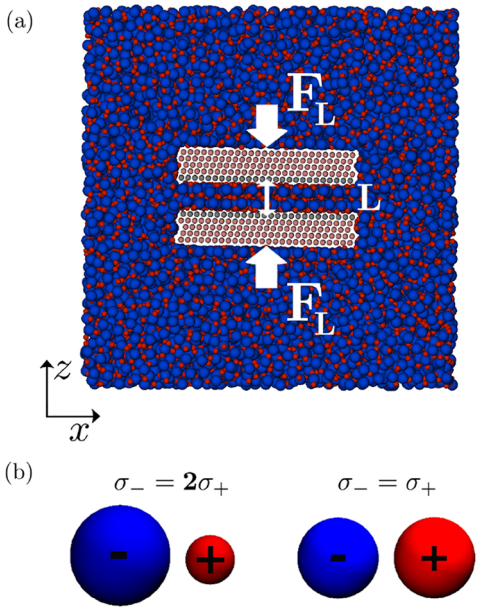

Figure 1. MD simulations. (a) Snapshot of the asymmetric IL immersing two charged surfaces in a fully periodic simulations box. The surfaces are pushed together along the z-direction with a normal force F_L to ultimately calculate the pressure as a function of the separation distance, L. (b) The ionic sizes, characterized by the LJ diameter, σ_i, for the (left) asymmetric and (right) symmetric systems.

https://doi.org/10.1021/acs.jpcb.1c09441
J. Phys. Chem. B 2022, 126, 1242−1253

concentration of both anions and cations in the simulation box is c_0 = 4.586 M and the absolute temperature is T = 600 K (usually elevated temperature is taken when "experimenting" with charged LJ-spheres, because at room temperature the dense plasma of such spheres freezes out). In our model, we account for the electronic polarizability of the ions in an effective manner. For this, we have set the background permittivity to be $\epsilon = 2\epsilon_0$,[52,53] where ϵ_0 is the permittivity of free space, with each ion possessing one elementary charge. The ions interact through LJ and Coulombic potentials, where the size asymmetry of the ions is controlled by adjusting their diameters through the LJ parameter σ_{ij} for species i interacting with species j, or σ_i when $i = j$. The ion sizes that we consider here for the asymmetric system are σ_- = 0.7 nm and σ_+ = 0.35 nm, and the ion size for the symmetric system is $\sigma_- = \sigma_+$ = 0.58 nm, such that the filling fraction is approximately equal in both systems, making $\sum_i \sigma_i^3 c_0$ unchanged. We also include attractive dispersion interactions. This is done in order to capture a more realistic representation of the IL, as these attractive dispersion interactions are active in real ILs. In our simulations, the cutoff distance of the LJ potential is set to be as long as 1.8 nm. Even so, as reaffirmed in the theoretical predictions which do not incorporate dispersion interactions, the main balance guiding the structural forces is the interplay between the ionic charge and ionic finite size.

Two parallel plates in the $x-y$ plane are immersed in a bulk of IL. We consider flat surfaces comprising LJ spheres in contact with the confined liquid, and a lattice parameter of mica.[52] Performing constant charge simulations, the surface charge on each plate is varied between $q_s = -0.12$ C/m^2 and $q_s = +0.12$ C/m^2. In the simulations, the image charge interactions are not taken into account. Simulations of IL nanofilms (1−10 nm thick) showed that the effect of electrode polarizability (image charges) on the vertical and lateral structure of the confined liquids is insignificant at practically feasible applied voltages.[54−56] Image charge interactions can lead, in principle, to the depletion of ions in the nanogap for a single layer of ions confined between two uncharged or slightly charged dielectric walls, as the ions, instead of "seeing" their counterions nearby, see their own weak images in the side walls (the situation may be different for metallic surfaces[57]). However, for larger separation distances between the surfaces, there is a weak dependence of the IL's structuring on the electrode polarizability which is explained by the screening of image charge interactions by the first layer of ions.[58] Therefore, in our work, we choose not to include image charge interactions, as we are particularly interested in isolating the structural layering of the liquid, which occurs even without the complexity that is added with the introduction of image charge interactions.

In the simulations, for each fixed surface charge the ionic density profiles between the surfaces are computed at a fixed separation distance, and the separation distance is varied to generate a pressure curve. Expansion on the simulation details and the used methods can be found further in the Supporting Information (SI).

2.2. Theoretical Derivation. The theory is based on an approximation of the Helmholtz free energy of a system of an asymmetric, hard-sphere 1:1 electrolyte with a constant background permittivity, ϵ, the primitive model.[34,59−61] The phenomenological basis for the theory is that the electrostatic and hard sphere components of the free energy of the system can be expressed in terms of locally homogenized quantities of the ion densities, the weighted-density approximation (WDA). The distinguishing feature of this model, as opposed to other similar classical DFT approaches,[62] is that the electrostatic contribution to the free energy is directly expressed in terms of weighted ionic densities.[22,63,64] The model is a generalization of the density functional for ILs presented in ref 22.

The core ingredients of the theory that allow us to capture the discrete layering in ILs are (i) representing the ions as delocalized shells of charge in their electrostatics and (ii) encoding the hard sphere packing of ions in their excess chemical potential. While these effects introduce some mathematical complexity, they have straightforward physical interpretations and do allow for some analytical progress, especially in the linear response limit.

To start, the free energy of the system can be broken down into three contributions, an ideal part $\mathcal{F}^{id}$, an excess part $\mathcal{F}^{ex}$, and an electrostatic part $\mathcal{F}^{el}$:

$$\mathcal{F} = \mathcal{F}^{id} + \mathcal{F}^{ex} + \mathcal{F}^{el} \tag{1}$$

The ideal contribution is related to the entropy of an ideal gas:

$$\mathcal{F}^{id}[\{c_i(\mathbf{r})\}] = \sum_i k_B T \int d\mathbf{r}\, c_i(\mathbf{r})[\ln(\nu_i c_i(\mathbf{r})) - 1] \tag{2}$$

where $k_B T$ is the thermal energy, ν_i is the volume of ion i, and c_i is the number density of ion i. For the hard sphere contribution to the free energy, we incorporate a phenomenological, simplified version of the Fundamental Measure Theory (FMT).[65] The advantage of our approach is that more compact expressions can be derived for the ionic excess chemical potential in terms of fewer weighting functions, aiding in the process of deriving simplified analytical approximations to the theory.

The phenomenological excess free energy we define is given by

$$\mathcal{F}^{ex}[\overline{c}_i(\mathbf{r})] = \frac{k_B T}{\hat{\nu}} \int d\mathbf{r} \left[\frac{1}{1-\overline{p}} - 3\overline{p} + \frac{1}{(1-\overline{p})^2} \right] \tag{3}$$

where $\overline{p}$ is the weighted volumetric filling fraction,

$$\overline{p} = \sum_i \nu_i w_{\nu,i} * c_i$$

$$w_{\nu,i}(\mathbf{r} - \mathbf{r}') = \frac{1}{\nu_i}\Theta(R_i - |\mathbf{r} - \mathbf{r}'|) \tag{4}$$

where R_i is the effective hard-sphere radius of the ion, $\nu_i = 4\pi R_i^3/3$ is the volume of the ion, the asterisk $(*)$ denotes a convolution, $w_{\nu,i}$ is the volumetric weighting function, Θ represents the Heaviside step function, and the filling-fraction-weighted volume $\hat{\nu}$ is given by

$$\hat{\nu} = \frac{\sum_i \nu_i^2 c_{i,0}}{\sum_i \nu_i c_{i,0}} = \frac{\sum_i \nu_i^2 c_{i,0}}{\eta} \tag{5}$$

Here, $c_{i,0}$ is the bulk concentration of species i and η is the bulk filling fraction, $\eta = \sum_i \nu_i c_{i,0}$. By construction, the key criteria that the simplified form of the hard sphere excess free energy satisfies are: (i) it retains the Carnahan−Starling equation of state[66] for the limit of symmetric ions or where one ionic species becomes vanishingly small while the other is of finite size, and (ii) it maintains the same singularities as the FMT functional.

https://doi.org/10.1021/acs.jpcb.1c09441
J. Phys. Chem. B 2022, 126, 1242−1253

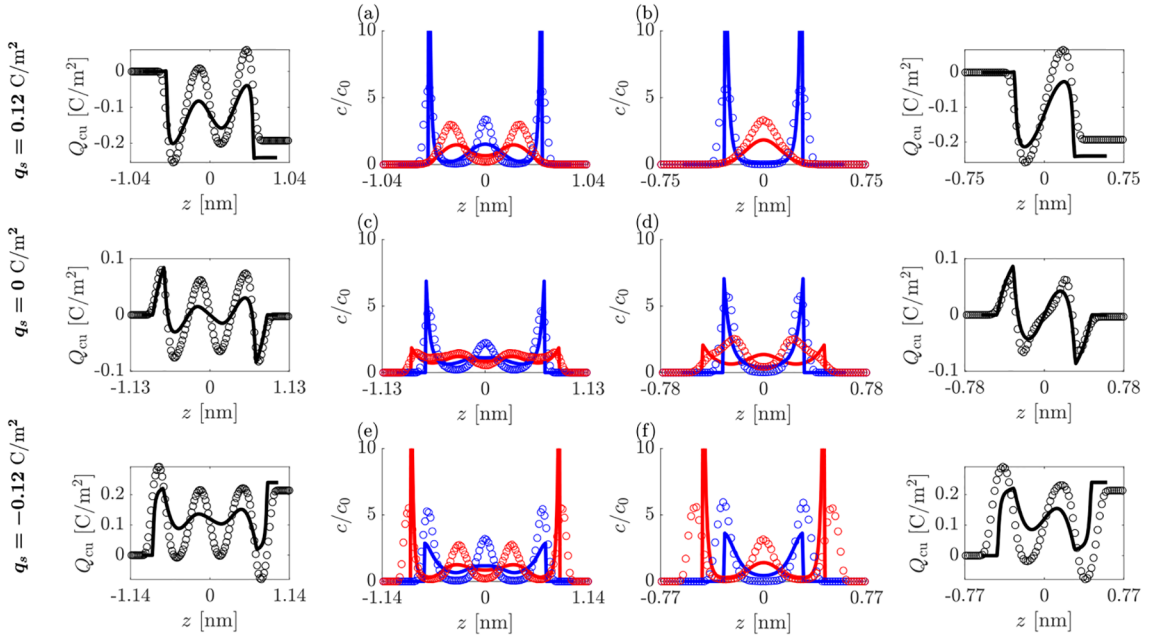

Figure 2. Charge and ion density profiles in asymmetric ILs between the charged plates. Rows correspond to the fixed surface charge densities of (a,b) q_s = 0.12 C/m^2, (c,d) q_s = 0 C/m^2, and (e,f) q_s = −0.12 C/m^2. Columns correspond to the squeeze out of a central electroneutral layer between two stable states where (a,c,e) $L \approx 2.2$ nm and (b,d,f) $L \approx 1.5$ nm. Cumulative charge functions are plotted to the left or right of the corresponding concentration profile plot. Markers (○) simulations; lines (—) theory. Color coding: blue, anions; red, cations.

The electrostatic part of the free energy in a medium with dielectric constant ϵ is expressed in terms of the electrostatic potential, ϕ, and the homogenized charge density, $\overline{\rho}_e$:[22]

$$\mathcal{F}^{\mathrm{el}}[\overline{\rho}_e, \phi] = \int \mathrm{d}\mathbf{r} \left\{ -\frac{\epsilon}{2}(\nabla\phi)^2 + \overline{\rho}_e \phi \right\} \tag{6}$$

This corresponds to the modified form of the Poisson equation, via minimization of the functional with respect to the electrostatic potential, $\delta\mathcal{F}/\delta\phi = 0$:

$$\epsilon\nabla^2\phi = -\overline{\rho}_e = -\sum_i z_i e c_i * w_{s,i}$$

$$w_{s,i}(\mathbf{r} - \mathbf{r}') = \frac{1}{4\pi R_i^2}\delta(R_i - |\mathbf{r} - \mathbf{r}'|) \tag{7}$$

where z_i is the valency of ion i, e is the elementary charge, and $\delta()$ denotes the delta function of 1D argument, such that each ionic weighting function $w_{s,i}$ corresponds to homogenizing over the surface of the ionic spheres. The weighted ionic concentrations signify that the ions act as shells of charge that interact with the local electrostatic potential.

Minimizing the free energy functional with respect to concentration, the ion densities at equilibrium satisfy:

$$c_i = c_{i,0} \exp(-z_i\beta e w_{s,i} * \phi - \beta w_{v,i} * \mu_i^{\mathrm{ex}} + \beta\mu_{i,b}^{\mathrm{ex}}) \tag{8}$$

where β is the inverse thermal energy and the excess chemical potential, μ_i^{ex}, is defined as

$$\beta\mu_i^{\mathrm{ex}} = \frac{\nu_i}{\hat{\nu}} \frac{8\overline{p} - 9\overline{p}^2 + 3\overline{p}^3}{(1-\overline{p})^3} \tag{9}$$

taking on a value in the bulk, $\mu_{i,b}^{\mathrm{ex}}$, of

$$\beta\mu_{i,b}^{\mathrm{ex}} = \frac{\nu_i}{\hat{\nu}} \frac{8\eta - 9\eta^2 + 3\eta^3}{(1-\eta)^3} \tag{10}$$

We again note that $\nu_i = \hat{\nu}$ for the case where (i) the two ions have the same size or (ii) when one ion is vanishingly small while the other has finite size. These limits give the standard expression for the Carnahan−Starling equation of state. For asymmetric ILs in which the ions both have significant packing effects, the formula effectively interpolates between these two limits.

We solve the above coupled integro-differential eqs 7 and 8 for the ionic densities and electrostatic potential between two flat electrodes, with equal surface charge density, q_s. In this case, the standard boundary condition for the potential is applied $\hat{\mathbf{n}}\cdot\epsilon\nabla\phi|_s = -q_s$. In the theory, the surface is assumed to be perfectly flat and hard with smeared charge density. In the theory, the representative surfaces are defined at $z = \pm L/2 \mp R_s$, where L is the distance between surface atom centers in the simulation and R_s is the surface atom radius. Therefore, the theoretical ionic densities are zero for $z < -L/2 + R_s + R_i$ and $z > L/2 - R_s - R_i$. We solve for the area averaged density, and we therefore reduce all equations to be dependent on one coordinate, z.[22] Numerically, we discretize the equations by a finite difference scheme.

For consistency between the simulations and theory, we need to define the ion diameter in the theory, d_i, as compared to the σ_{ij} values of the simulation. Since the LJ interaction is not exactly the same as the hard sphere interaction assumed in the theory, the ions in the simulation can overlap slightly with the surface and with each other below a center-to-center separation of σ_i. We assume that the effective ionic diameter in the theory is set by a cutoff criterion, where the LJ potential is $U_{\mathrm{LJ}} = 0.3k_{\mathrm{B}}T$, corresponding to $d_i \approx 0.9\sigma_i$. The sensitivity of the results with respect to this criterion is discussed in the SI.

The pressure between the two equally charged surfaces as a function of separation distance is calculated as[67−70]

$$P = -\frac{\delta(\Omega/A)}{\delta L} \tag{11}$$

https://doi.org/10.1021/acs.jpcb.1c09441
J. Phys. Chem. B 2022, 126, 1242−1253

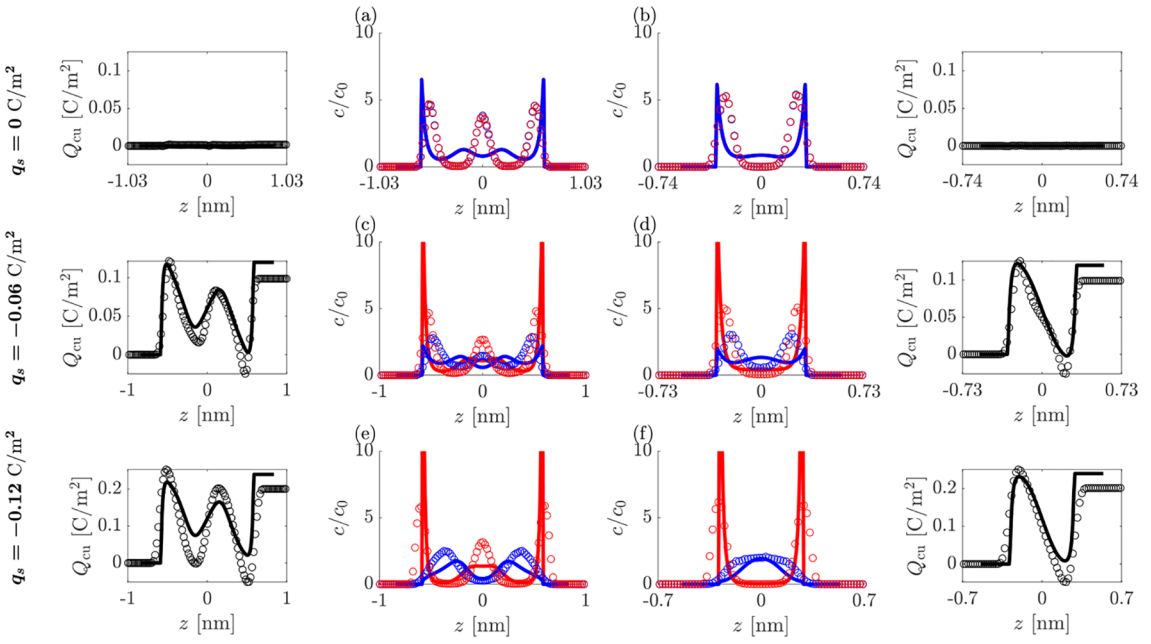

Figure 3. Charge and ion density profiles in symmetric IL. Rows correspond to the fixed surface charge of (a,b) $q_s = 0$ C/m^2, (c,d) $q_s = -0.06$ C/m^2, and (e,f) $q_s = -0.12$ C/m^2. Columns correspond to the squeeze out of a central electroneutral layer between two stable states where (a,c,e) $L \approx 2$ nm and (b,d,f) $L \approx 1.4$ nm. Cumulative charge functions are plotted to the left or right of the corresponding concentration profile plot. Markers (○) simulations; lines (—) theory. Color coding: blue, anions; red, cations.

at constant temperature and reference chemical potential (constant bulk ionic concentrations), where A is the area of the surfaces, and Ω is the grand potential

$$\Omega = \mathcal{F} - \sum_i \int d\mathbf{r}\{\mu_{i,b} c_i\} \tag{12}$$

and $\mu_{i,b}$ is the bulk chemical potential. By definition, the pressure corresponds to the change in the grand potential per differential change in the system volume, assuming fixed area of the confining surfaces. The values of Ω/A for a range of separation distances are numerically computed, and we then numerically differentiate this function to calculate the disjoining pressure. The zero value for the disjoining pressures corresponds to the bulk reference value as $L \to \infty$, $P_\infty = 0$.

3. RESULTS AND DISCUSSION

3.1. Ionic Charge and Density Profiles. We start by comparing in Figure 2 the ionic densities calculated from the simulations (circles, ○) and theory (lines, —) as the ionic layers are squeezed out (columns, panels a–f) at varying surface charge/polarities (rows). Beyond simply plotting the density of ionic centers, c_i, layering is demonstrated by plotting the cumulative charge (accompanying plots to the left and right of panels a–f), with the cumulative charge function, $Q_{cu}(z)$, defined as

$$Q_{cu}(z) = \int_{-L/2}^{z} \sum_i z_i e c_i(z')\, dz' \tag{13}$$

Figure 2 shows that the theory captures the main features of the charge ordering found in the simulations, particularly when plotted in terms of $Q_{cu}(z)$. However, the theory does not accurately predict the magnitude of the overscreening as the separation distance increases, and underpredicts the decay into the bulk for the widest separations. Interestingly, the theory is more in line with simulations when describing the charge ordering at small separations between the plates, where the bulk correlations of the ions are the least influential.

The main discrepancies between the theory and simulations are the sharpness and magnitude of the ionic density peaks, arising because the theory assumes hard-sphere interactions while the simulations assume LJ interactions. Further, whereas the theory obeys electroneutrality within the space between the two charged surfaces ($Q_{cu}(z = L/2) = -2q_s$), the simulations exhibit some partial charge screening from the IL outside the gap, so that $Q_{cu}(z = L/2) \neq -2q_s$.

Inspecting the density profiles in Figure 2, we can see that at zero surface charge (panels c and d), both the theory and the simulations show that the smaller ion, the cation in our study (displayed in red color), can access the surface more easily. For negatively charged surfaces (panels e and f), the small cation concentration is enhanced drastically near the surfaces, yet the same number of layers are maintained as in the zero charge case. At a positive surface charge (panels a and b), the cation is pushed out of the region closest to the surfaces, resulting in fewer layers of ions in this limit.

We can then contrast the screening with asymmetric ions to screening with symmetric ions. In Figure 3, the ionic density profiles for the symmetric system are shown, for increasing negative surface charge and two separation distances. Since a change in the surface polarity gives identical profiles (up to the identity of the symmetric ions) only negative surface charge values are shown. Again, overall, the theory captures ordering in charge and density between the charged surfaces quite well, with close agreement for the smallest separation distances. At zero surface charge (panels a and b), here, unlike the asymmetric ionic system, no local ionic charge density occupies the gap, since neither ion preferentially accesses the surface. The ions then form overlapping layers, which turn into alternating ones when increasing the surface charge (panels c–f). Overall, the overscreening structure remains similar as the

https://doi.org/10.1021/acs.jpcb.1c09441
J. Phys. Chem. B 2022, 126, 1242−1253

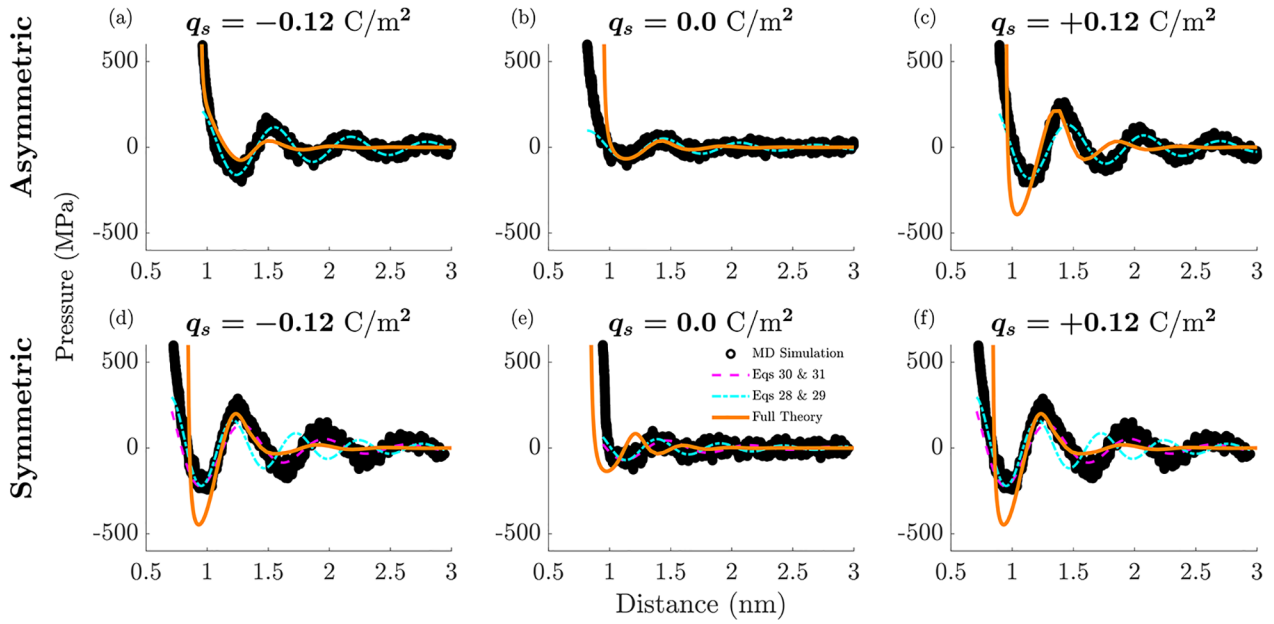

Figure 4. Disjoining pressure profiles. (a–c) Asymmetric system and (d–f) symmetric system for (a,d) negative, (b,e) uncharged, and (c,f) positive surfaces. The black markers (○) are the MD simulation data points. The solid orange lines are the full, nonlinear integro-differential theory. The other dashed and dash-dot lines are applications of the approximation in eq 14, where the parameters P_0 and z_0 are fit only to the first minimum. Here, the cyan dash-dot lines correspond to the analytical expressions for κ in eqs 28 and 29, while the magenta dashed lines plotted in (d–f) correspond to the definitions in eqs 30 and 31. These equations are derived in the framework of the linear response analysis.

surface charge magnitude increases, since the surface charges tested are not large enough to enter the crowding regime.

Thus, after comparing the density profiles between confined asymmetric and symmetric ionic systems we find that the most pronounced effect for the asymmetric ionic system is an entropy-driven preferential adsorption of smaller ions which emerges even at zero surface charge of the electrodes. This spontaneous layering of charges near the zero charged electrodes is completely nontrivial and it essentially emphasizes the strong effect that the ionic size asymmetry has on the layering structure of positive and negative charges near flat charged interfaces. Additional charge and density profiles with varying surface charges and separation distances for both the asymmetric and symmetric systems are presented in the SI.

3.2. Disjoining Pressure Profiles. *3.2.1. Simulations and Integro-differential Theoretical Results.* Finally, the role of ionic asymmetry on structural forces is demonstrated in Figure 4. Pressure profiles are plotted as a function of the surface separation distance for the asymmetric (panels a–c) and symmetric (panels d–f) systems, where they are confined between negatively (panels a and d), uncharged (panels b and e), and positively charged surfaces (panels c and f). Additional results with varying surface charge magnitudes are presented in the SI. Comparing the theory to the simulations, overall, there is an agreement between the MD simulation pressure profiles (black markers ○ in Figure 4) and the full integro-differential results from the theory (solid orange lines in the top and bottom rows, the asymmetric and symmetric systems, respectively). This agreement is most pronounced at the smallest separation distances, where the pressure magnitudes are the most significant. The main discrepancy, as similarly noted already for the ionic density profiles, is that the oscillations decay more quickly for the theory than those that are observed in the simulations.

While the pressure profiles in Figure 4 appear to be similar for both systems, there are still significant differences with respect to surface charge magnitude and sign. Referring specifically to the simulated pressure profiles (black markers ○ in Figure 4), as expected, the amplitude of the pressure oscillations increases as the surface charge magnitude increases for both the asymmetric and the symmetric systems. However, for the asymmetric system, the pressure oscillation amplitudes are larger for the positive surface charge polarity, due to the larger anions accumulating between the positively charged surfaces. Meanwhile, as expected, the pressure profiles for the symmetric system do not depend on the sign of the surface charge density. In the asymmetric system, the period of oscillation is not affected by the electrode polarity or magnitude. This is because at small potential drops across the double layer, overscreening is always present, and the overscreening period and decay are determined by the diameter of the larger ion. For the symmetric system, the period of the pressure oscillations increases slightly at $q_s = \pm 0.12$ C/m^2, yet it still remains on the scale of an individual ionic diameter.

The theory in general also captures these features, particularly the asymmetric pressure response of the asymmetric IL with changing surface polarity, as well as the oscillation period, being on the order of the largest ionic diameter (orange lines in Figure 4a–c).

3.2.2. Linear Response Analysis. To gain further insight into the differences between the pressure profiles of the symmetric and asymmetric systems, we seek an approximate theoretical description in which the pressure profiles are represented by an exponentially decaying oscillating form,

$$P = P_0\, e^{-\kappa_1(z-z_0)} \cos(\kappa_2(z - z_0)) \tag{14}$$

where κ_1 encodes the decay length of oscillations while κ_2 encodes the period of oscillations. Approximating the theory at

https://doi.org/10.1021/acs.jpcb.1c09441
J. Phys. Chem. B 2022, 126, 1242–1253

a linear response, the values for κ_1 and κ_2 are determined from the decay modes in the charge density, which is proportional to $c_+ - c_-$, and the total number density $c_+ + c_-$. While the equations presented thus far are generally nonlinear integro-differential equations, in the limit of small, slowly varying perturbations in linear response to the charge of the surfaces, we can derive analytical formulas to approximate the oscillatory decay of the charge and number density as a function of the IL properties. Here, we present the detailed derivation and analysis of the approximations involved in the linear response theory.

Limit of small perturbations: Equation 8 for small perturbations in the linear response can be approximated as

$$c_i \approx c_{i0}(1 - z_i e\beta w_{si} * \phi - \beta w_{vi} * \mu_i^{ex} + \beta\mu_{i,bulk}^{ex}) \tag{15}$$

The excess chemical potential can be linearized to give:

$$\begin{aligned}\beta\mu_i^{ex} &= \frac{v_i}{\hat{v}}\frac{(8\bar{p} - 9\bar{p}^2 + 3\bar{p}^3)}{(1-\bar{p})^3} \\ &\approx \beta\mu_{i,bulk}^{ex} + \frac{v_i}{\hat{v}}\frac{2(4-\eta)}{(1-\eta)^4}(\bar{p} - \eta)\end{aligned} \tag{16}$$

where we have linearized the weighted filling fraction $\bar{p}$, with reference value given by the bulk filling fraction, η. Therefore, if we assume linear perturbations of the bulk state, where $\delta f = f - f_b$, we have the following coupled equations for the linearized Poisson equation and the ionic concentrations:

$$\delta c_i \approx -z_i c_{i0} e\beta w_{si} * \phi - \frac{v_i c_{i0}}{\hat{v}}\frac{2(4-\eta)}{(1-\eta)^4} w_{vi} * \sum_j v_j w_{vj} * \delta c_j \tag{17}$$

$$\epsilon\nabla^2\phi = -\sum_i z_i e w_{si} * \delta c_i \tag{18}$$

In the proceeding equations, we will analyze the decaying modes for these differential equations for the cases of (i) the symmetric IL system and (ii) the asymmetric IL system. We briefly comment on (iii) systems with only a small degree of size asymmetry. In each of these analyses, we will use the following differential approximation for the convolution integrals, derived by truncating the Fourier transform of the convolution operations for small perturbations,[22] giving

$$w_{vi} * \delta f \approx (1 + l_{vi}^2\nabla^2)\delta f \tag{19}$$

$$w_{si} * \delta f \approx (1 + l_{si}^2\nabla^2)\delta f \tag{20}$$

where l_{vi} and l_{si} are determined by the ionic size:

$$l_{vi} = \frac{d_i}{\sqrt{40}} \tag{21}$$

$$l_{si} = \frac{d_i}{\sqrt{24}} \tag{22}$$

where the numerical values of $\sqrt{40}$ and $\sqrt{24}$ are given directly from the mathematical form of the weighting functions.

The symmetric case: For the symmetric case, $w_{si} = w_s$, $w_{vi} = w_v$, and $v_i = \hat{v}$. The linear response for the symmetric system was reported previously,[22] but we again go through the process in order to draw contrast with the asymmetric case. For a 1:1 IL, we get the following:

$$\delta c_+ \approx -c_0 e\beta w_s * \phi - \nu c_0\frac{2(4-\eta)}{(1-\eta)^4} w_v^2(\delta c_+ + \delta c_-) \tag{23}$$

$$\delta c_- \approx c_0 e\beta w_s * \phi - \nu c_0\frac{2(4-\eta)}{(1-\eta)^4} w_v^2(\delta c_+ + \delta c_-) \tag{24}$$

$$\epsilon\nabla^2\phi = -e w_s * \delta c_- - w_s * \delta c_+ \tag{25}$$

If we sum the first two expressions and multiply by v, we get:

$$\delta p = \sum_i \nu\delta c_i \approx -\frac{2\eta(4-\eta)}{(1-\eta)^4} w_v^2\delta p \tag{26}$$

where again, $p = v\sum_i c_i$ is the local filling fraction. Next, if we subtract the first two expressions and substitute into the third equation, we get

$$\epsilon\nabla^2\phi = 2e^2\beta c_0 w_s^2\phi \tag{27}$$

Here, we see that the equations for the potential and filling fraction at linear response are decoupled for the symmetric system. For the case where all functions become a function of z only, we can trial the solution $\delta f = A\exp(-\kappa z)$ to find the values for the decaying modes, κ. For the equation governing the filling fraction, $\delta p = A_m\exp(-\kappa_m z)$, (directly proportional to the total number density) the decay has both a real and imaginary part, where

$$\kappa_{1m} = \mathrm{Re}(\kappa_m) = \frac{\sqrt{40}}{d}\sqrt{-\frac{1}{2} + \frac{1}{2}\sqrt{1 + \frac{(1-\eta)^4}{2\eta(4-\eta)}}} \tag{28}$$

$$\kappa_{2m} = \mathrm{Im}(\kappa_m) = \pm\frac{\sqrt{40}}{d}\sqrt{\frac{1}{2} + \frac{1}{2}\sqrt{1 + \frac{(1-\eta)^4}{2\eta(4-\eta)}}} \tag{29}$$

The decay in number density is always oscillatory for nonzero filling fraction, since as $\eta \to 0$, $\kappa_{1m} \approx \kappa_{2m} \approx d^{-1}(\eta/50)^{-1/4}$. On the other hand, as $\eta \to 1$, the number density profile becomes purely oscillatory (without decay) with a period of oscillation close to the ion diameter.

Next, for the equation governing the electrostatic potential in the limit of high ionic concentration, with trial solution $\delta\phi = A_c\exp(-\kappa_c z)$, the decaying mode has different real and imaginary components:

$$\kappa_{1c} = \mathrm{Re}(\kappa_c) = \frac{12\lambda_D}{d^2} \tag{30}$$

$$\kappa_{2c} = \mathrm{Im}(\kappa_c) = \pm\frac{12\lambda_D}{d^2}\sqrt{\frac{d^2}{6\lambda_D^2} - 1} \tag{31}$$

where λ_D is the Debye length.

Even in linear response, we see that the two decaying modes will compete with one another in determining the overall disjoining pressure for the symmetric system. Both have similar nanometric decay ranges in the concentrated limit of ILs. At high charge density, the mode governing the decay of charge will dominate, κ_c. At low charge density, the decay of charge is unimportant in the double layer structure, so the decay in the number density (and packing fraction), κ_m will dominate.

The asymmetric case: For the asymmetric system, it is more difficult to make analytical progress in solving for the decaying modes. First and foremost, the decay in number density

https://doi.org/10.1021/acs.jpcb.1c09441
J. Phys. Chem. B 2022, 126, 1242−1253

(packing fraction) is coupled explicitly to the decay in charge density (potential). This fact arises because of the differences in the excess chemical potential between the different ions, which do not allow for the neat cancellations encountered with the symmetric system.

Further, even in solving the general problem for the decaying modes for each ionic species and the potential, analytical progress toward simple formulas is burdensome. For that reason, we will perform analysis for the limit of perfect asymmetry $d_- \gg (d_+ \approx 0)$ and high packing fraction. Then the governing linear response equations can be reframed as

$$\delta c_+ \approx -c_0 e\beta\phi \tag{32}$$

$$\delta c_- \approx c_0 e\beta w_{s-} * \phi - \nu_- c_0 \frac{2(4-\eta)}{(1-\eta)^4} w_{\nu-}^2 \delta c_- \tag{33}$$

$$\epsilon\nabla^2\phi = -e\delta c_+ + w_{s-} * e\delta c_- \tag{34}$$

By substitution for ϕ and δc_+ into the equation for the potential, we get a single characteristic equation for the anion concentration decay:

$$\left[1 + \frac{2\eta(4-\eta)}{(1-\eta)^4} w_{\nu-}^2\right]\nabla^2\delta c_- = \frac{\kappa_D^2}{2}\left[1 + w_{s-}^2 + \frac{2\eta(4-\eta)}{(1-\eta)^4} w_{\nu-}^2\right]\delta c_- \tag{35}$$

Now, we can simplify this linearized expression by taking limits of κ_D, in relation to the characteristic length scale of the gradients in concentration, which is the ionic diameter d_- at high concentration.

As a quick side note, the limit of $d_- \to 0$ where $w_{s-} \approx 1$ gives the Debye−Huckel linearized form:

$$\nabla^2\delta c_- = \kappa_D^2 \delta c_- \tag{36}$$

so dilute electrolytes still have the Debye length (as it should be) as characteristic decay length, as long as the filling fraction η in the electrolyte is near zero.

If $\kappa_D d_- \ll 1$ and $\eta \neq 0$, then we get the following leading sixth order differential equation for δc_-:

$$\left[1 + \frac{2\eta(4-\eta)}{(1-\eta)^4} w_{\nu-}^2\right]\nabla^2\delta c_- = 0 \tag{37}$$

valid near the interface. The more relevant limit to concentrated ILs is when $\kappa_D d_- \to \infty$, which at the leading order of eq 35 gives

$$\left[1 + w_{s-}^2 + \frac{2\eta(4-\eta)}{(1-\eta)^4} w_{\nu-}^2\right]\delta c_- = 0 \tag{38}$$

For the purpose of simplicity, we can assume roughly that $w_{s-} \approx w_{\nu-}$. Next, at the filling fraction in the given parameter space, it is safely assumed that the term involving η dominates the differential equation at a large filling fraction, such that the form of the equation can be approximated as

$$\left[1 + \frac{2\eta(4-\eta)}{(1-\eta)^4} w_{\nu-}^2\right]\delta c_- \approx 0 \tag{39}$$

In the limit of large filling fraction and perfect asymmetry, the longest decaying mode governing the decay of the ionic concentration can be approximated by κ_m, again with its real and imaginary components:

$$\kappa_{1m} = \mathrm{Re}(\kappa_m) = \frac{\sqrt{40}}{d_-}\sqrt{-\frac{1}{2} + \frac{1}{2}\sqrt{1 + \frac{(1-\eta)^4}{2\eta(4-\eta)}}} \tag{40}$$

$$\kappa_{2m} = \mathrm{Im}(\kappa_m) = \pm\frac{\sqrt{40}}{d_-}\sqrt{\frac{1}{2} + \frac{1}{2}\sqrt{1 + \frac{(1-\eta)^4}{2\eta(4-\eta)}}} \tag{41}$$

Here, the asymmetric system has one main decaying mode, owing to the coupling of oscillations in charge and number density. As $\eta \to 1$, the anion concentration profile becomes purely oscillatory with period roughly equal to the anion diameter, corresponding to a crystal of densely packed anions.

Small degrees of asymmetry: One important question is whether there is a smooth transition between the symmetric behavior and the asymmetric behavior depending on the extent of asymmetry. The degree of coupling between the charge density and total number density can be determined via the linear response equations. As a starting point, we consider the sum of the linear equations for the cation and anion, $\delta c_+ + \delta c_-$:

$$\delta c_+ + \delta c_- \approx c_0 e\beta(-w_{s+} + w_{s-}) * \phi - \frac{(\nu_+ w_{\nu+} + \nu_- w_{\nu-})c_0}{\hat{\nu}} \frac{2(4-\eta)}{(1-\eta)^4} * \sum_j \nu_j w_{\nu j} * \delta c_j \tag{42}$$

The coupling of the charge density decay with the number density decay is controlled by the term containing ϕ. From this term, we observe that the system is decoupled when $w_{s+} \approx w_{s-}$, or in terms of the approximate differential operators, $1 + d_+^2/24\nabla^2 \approx 1 + d_-^2/24\nabla^2$. From these relationships, we find that decoupling occurs when $d_+ \approx d_-$, for symmetric ion sizes. Approximately, the extent of asymmetry can be quantified using the difference in differential operators, $w_{s-} - w_{s+}$, assuming gradients on the order of the smallest length scale in the system, the smallest ion size (d_+ in this case). Therefore, the system will reproduce perfect asymmetric behavior when

$$\frac{|d_-^2 - d_+^2|}{d_+^2} \gg 1 \tag{43}$$

and will reproduce perfect symmetric behavior when:

$$\frac{|d_-^2 - d_+^2|}{d_+^2} \ll 1 \tag{44}$$

Therefore, according to the linear response to small perturbations in the theory, systems with only slight asymmetry will behave similar to the symmetric system if they satisfy eq 44.

Summary of linear response results: In the linear response regime, we find that the charge density oscillations in the symmetric system are independent of the number density oscillations, as they are decoupled from each other. However, in the asymmetric system, in the linear response, consistent with our explanation for the results of the simulations and the full integro-differential theory, we find that the period (as well as the decay length) of oscillations in both charge and number density is determined by the diameter of the larger ion, and so the two are coupled to each other.

https://doi.org/10.1021/acs.jpcb.1c09441
J. Phys. Chem. B 2022, 126, 1242−1253

For the asymmetric system, in the limit of large filling fraction and perfect asymmetry, the longest decay mode in charge and number density can be approximately described by the definitions of κ_{1m} and κ_{2m} as derived above in eqs 40 and 41. Therefore, for the asymmetric system, this mode dominates the value of the disjoining pressure at all surface charges. The decay of oscillations in this high packing fraction limit is independent of the background permittivity and ionic charge. This is because in the regime of high packing, the structure and correlations in the system are determined majorly by the steric dense packing constraints, valid if $\kappa_{1m} \ll \kappa_D$.

For the symmetric system, as mentioned above, the ordering in charge and number density are decoupled. For this case, the number density decays with modes described by κ_{1m} and κ_{2m} in eqs 28 and 29, similarly to eqs 40 and 41, since these formulas are generally applicable for the decay in number density in a dense fluid at a hard wall. In contrast, the charge density decays as given by the definitions for κ_{1c} and κ_{2c} in the highly concentrated limit by eqs 30 and 31. For the symmetric system at low surface charge, the oscillations in charge are less pronounced than the oscillation in the number density, so the decay in the number density (and filling fraction), κ_m, will dominate in determining the pressure profile. Alternatively, at high surface charge, the mode governing the decay of charge, κ_c, will dominate. One could expect similar trends for ions that are only approximately symmetric in size, with only a small degree of asymmetry. Therefore, as $\nu_- \rightarrow \nu_+$, there is a transition between the perfectly asymmetric and the perfectly symmetric behaviors, as analyzed in the linear response behavior above.

We present our findings for both the symmetric and asymmetric systems in Figure 4, where the approximations corresponding to eq 14 with κ_m as given in eqs 28 and 29, and κ_c as given in eqs 30 and 31 are plotted, manually fitting the point of the first minimum of the simulation data with P_0 and z_0, but keeping all other analytical formulas above. The decay decrement, κ_m, governed by the filling fraction is plotted with the dashed-dot cyan lines, while the decay decrement, κ_c, governed by the decay in charge is plotted with the dashed magenta lines.

For the asymmetric system (panels a−c), as mentioned above, κ_m describes the decay at all surface charges. Therefore, in Figure 4, one can observe that the dashed-dot cyan lines fitted to the first minimum compare almost perfectly at all surface charges to the pressure oscillations found in the simulations.

For the symmetric system, however, the decaying mode given by κ_m, plotted with the dashed-dot cyan lines, only dominates at zero surface charge (panel e). In contrast, since the decay in pressure oscillations at high electrode charges such as $q_s = \pm 0.12$ C/m^2 is dominated by the decrement, κ_c, the plotted dashed magenta lines in Figure 4, panels d and f, match better with the pressure oscillations found in the simulations at these high surface charges (one can see how the dashed-dot cyan line for κ_m is in offset and does not describe well the simulated pressure oscillations).

Seeing as how the approximate equations of the linear response theory describe quite accurately the decay of the simulated pressure, we can now compare and validate quantitatively the periodicities of the pressure oscillations displayed in Figure 4. In the simulations, the period of the first oscillation (distance from first to second minimum) in the asymmetric system for the surface charges of $q_s = -0.12$, -0.06, 0, +0.06, and +0.12 C/m^2 are 0.59, 0.62, 0.57, 0.60, and 0.61 nm, respectively. This compares well to the result from the linearized formula for κ_{2m} in eq 29, which predicts a period of 0.62 nm for the asymmetric system. This value is essentially the effective largest ionic diameter $d_i \approx 0.9\sigma_i$, where $\sigma_- = 0.7$ nm (our criterion that takes into account the overlap of ions in the simulations), showing numerically that the periodicity of oscillations in asymmetric systems at all surface charges is determined by the diameter of the larger ion. For the symmetric system, the simulated periods of the first oscillation for $q_s = 0$, ± 0.06, and ± 0.12 C/m^2 are 0.53, 0.58, and 0.66 nm, respectively. The periodicity values at low surface charges are given by κ_{2m} in eq 29, which predicts a period of 0.52 nm (again, $d_i \approx 0.9\sigma_i$, where $\sigma_\pm = 0.58$ nm). At high surface charge densities, the periodicity values are given by κ_{2c} in eq 31, which predicts a period of 0.68 nm, numerically showing the increase in the oscillation period with surface charge magnitude in this case.

We note that while in previous experimental measurements of surface forces in IL, the oscillation period has been described in terms of the ion pair diameter,[8,9,47,48] the oscillation period in the simulations and the theory presented here, at the high concentration limit, more closely matches the diameter of the largest ion, in all cases, multiplied by the scalar prefactor that is close to 1.

4. CONCLUSIONS

All in all, the change in the oscillatory decay as a function of surface charge underlies a major difference between charge screening in concentrated asymmetric systems compared to concentrated symmetric ones. In asymmetric systems, the decay modes in charge and number density are coupled to each other, and therefore give the same decay mode. For the symmetric system, the two are decoupled. This essentially leads to differences in the microscopic ionic concentration profiles in nanoconfinement as a function of electrode charge magnitude and polarity, and ultimately to an observable difference in the disjoining pressure profile. Our unraveled findings presented here provide some generalizable insights into the detailed behaviors of such concentrated ionic systems. These insights, therefore, may be taken into consideration in terms of the analytical expressions that are derived in our work, and can help interpret results of future experimental data of structural forces in ionic liquids, as well as simulations.

To summarize, the main novel scientific contribution of our work is our proposed continuum theory which describes well the density, charge distributions, and structural forces of ILs in nanoscale confinements and the effect of surface polarization on these quantities. Through application of this theory, we can relate the oscillation periodicity and decay of the molecular structuring and charge density oscillations in nanoconfinement to the physical properties of the IL, including the bulk ionic density, the ionic sizes, the temperature, and the background permittivity. While the MD simulations and theory profiles do not match perfectly, both approaches predict layered structures that lead to structural forces at small separation distances. Both simulations and theory also recover the main features of screening in asymmetric ILs, which are not present in symmetric ILs. Those include the variation of force amplitudes depending on the surface charge polarity, the "preferential adsorption" of smaller ions at zero electrode charge, and the coupling of charge and number density oscillations in systems at such high ionic concentration. Therefore, on the basis of our

https://doi.org/10.1021/acs.jpcb.1c09441
J. Phys. Chem. B 2022, 126, 1242−1253

findings, we conclude that the ionic size asymmetry is an important ingredient in describing ILs at the nanoscale.

■ ASSOCIATED CONTENT

Supporting Information

The Supporting Information is available free of charge at https://pubs.acs.org/doi/10.1021/acs.jpcb.1c09441.

Additional simulation details and results with varying theory parameters (PDF)

■ AUTHOR INFORMATION

Corresponding Author

Alexei A. Kornyshev − *Department of Chemistry, Molecular Sciences Research Hub, Imperial College London, London W12 0BZ 2AZ, United Kingdom; Thomas Young Centre for Theory and Simulation of Materials, Imperial College London, London SW7 2AZ, United Kingdom;* orcid.org/0000-0002-3157-8791; Email: a.kornyshev@imperial.ac.uk

Authors

J. Pedro de Souza − *Department of Chemical Engineering, Massachusetts Institute of Technology, Cambridge, Massachusetts 02139, United States;* orcid.org/0000-0003-3634-4991

Karina Pivnic − *School of Chemistry, The Sackler Center for Computational Molecular and Materials Science, Tel Aviv University, Tel Aviv 6997801, Israel*

Martin Z. Bazant − *Department of Chemical Engineering, Massachusetts Institute of Technology, Cambridge, Massachusetts 02139, United States; Department of Mathematics, Massachusetts Institute of Technology, Cambridge, Massachusetts 02139, United States;* orcid.org/0000-0002-8200-4501

Michael Urbakh − *School of Chemistry, The Sackler Center for Computational Molecular and Materials Science, Tel Aviv University, Tel Aviv 6997801, Israel;* orcid.org/0000-0002-3959-5414

Complete contact information is available at: https://pubs.acs.org/10.1021/acs.jpcb.1c09441

Author Contributions

⊥J.P.D. and K.P. contributed equally to this work.

Notes

The authors declare no competing financial interest.

■ ACKNOWLEDGMENTS

J.P.D., M.Z.B., and A.A.K. acknowledge support from the MIT-Imperial seed fund. J.P.D. and M.Z.B. acknowledge support from the Center for Enhanced Nanofluidic Transport, an Energy Frontier Research Center funded by the U.S. Department of Energy, Office of Science, Basic Energy Sciences under Award No. DE-SC0019112. J.P.D. also acknowledges support from the National Science Foundation Graduate Research Fellowship under Award No. 1122374. A.A.K. and M.U. acknowledge the award of a Research Grant by The Leverhulme Trust (RPG-2016- 223). K.P. and M.U. acknowledge the financial support of the Israel Science Foundation, Grant No. 1141/18, and of the Deutsche Forschungsgemeinschaft (DFG), Grant No. BA 1008/21.

■ GLOSSARY OF SYMBOLS

σ_i	LJ Parameter for the *i,i* interaction
F_L	normal force
L	plate separation distance
c_0	bulk ionic concentration
ϵ	background permittivity
ϵ_0	permittivity of free space
T	absolute temperature
q_s	surface charge density
$\mathcal{F}$	Helmholtz free energy
$\mathcal{F}^{\mathrm{Id}}$	ideal contribution to free energy
$\mathcal{F}^{\mathrm{ex}}$	excess contribution to free energy
$\mathcal{F}^{\mathrm{el}}$	electrostatic contribution to free energy
k_B	Boltzmann constant
c_i	concentration of species *i*
$\overline{p}$	weighted volumetric filling fraction
$\hat{v}$	weighted volume
v_i	ionic volume of species *i*
R_i	effective hard-sphere ionic radius of species *i*
$w_{v,i}$	volumetric weighting function
η	bulk filling fraction
$c_{i,0}$	bulk ionic concentration of species *i*
ϕ	electrostatic potential
$\overline{\rho}_e$	homogenized charge density
z_i	valency of ion *i*
e	elementary charge
$w_{s,i}$	surface weighting function
β	inverse thermal energy
μ_i^{ex}	excess chemical potential
$\mu_{i,b}^{\mathrm{ex}}$	bulk excess chemical potential
R_s	surface atom radius
d_i	effective hard-sphere ionic diameter of species *i*
U_{LJ}	LJ potential
P	pressure
A	area
Ω	grand potential
P_∞	reference pressure as $L \to \infty$
Q_{cu}	cumulative charge function
P_0	pressure at first minimum
z_0	separation distance at first minimum
κ_1	inverse decay length of pressure
κ_2	oscillation frequency of pressure
δf	linear perturbation function
f	local value of function
f_b	bulk reference value of function
l_{vi}	length scale for differential approximation of $w_{v,i}$
l_{si}	length scale for differential approximation of $w_{s,i}$
κ_{1m}	inverse decay length of total number density
κ_{2m}	oscillation frequency of total number density
κ_{1c}	inverse decay length of charge density (symmetric system)
κ_{2c}	oscillation frequency of charge density (symmetric system)
λ_{D}	Debye length
κ_{D}	inverse Debye length

■ REFERENCES

(1) Krossing, I.; Slattery, J. M.; Daguenet, C.; Dyson, P. J.; Oleinikova, A.; Weingärtner, H. Why are ionic liquids liquid? A simple explanation based on lattice and solvation energies. *J. Am. Chem. Soc.* **2006**, *128*, 13427−13434.

(2) Hallett, J. P.; Welton, T. Room-temperature ionic liquids: solvents for synthesis and catalysis. 2. *Chem. Rev.* **2011**, *111*, 3508−3576.
(3) Fedorov, M. V.; Kornyshev, A. A. Ionic Liquids at Electrified Interfaces. *Chem. Rev.* **2014**, *114*, 2978−3036.
(4) Palacio, M.; Bhushan, B. A review of ionic liquids for green molecular lubrication in nanotechnology. *Tribol. Lett.* **2010**, *40*, 247−268.
(5) Li, H.; Wood, R. J.; Rutland, M. W.; Atkin, R. An ionic liquid lubricant enables superlubricity to be "switched on" in situ using an electrical potential. *Chem. Commun.* **2014**, *50*, 4368−4370.
(6) Pivnic, K.; Bresme, F.; Kornyshev, A. A.; Urbakh, M. Electrotunable Friction in Diluted Room Temperature Ionic Liquids: Implications for Nanotribology. *ACS Appl. Nano Mater.* **2020**, *3*, 10708−10719.
(7) Atkin, R.; Warr, G. G. Structure in confined room-temperature ionic liquids. *J. Phys. Chem. C* **2007**, *111*, 5162−5168.
(8) Perkin, S. Ionic liquids in confined geometries. *Phys. Chem. Chem. Phys.* **2012**, *14*, 5052−5062.
(9) Krämer, G.; Hausen, F.; Bennewitz, R. Dynamic shear force microscopy of confined liquids at a gold electrode. *Faraday Discuss.* **2017**, *199*, 299−309.
(10) Pivnic, K.; Bresme, F.; Kornyshev, A. A.; Urbakh, M. Structural forces in mixtures of ionic liquids with organic solvents. *Langmuir* **2019**, *35*, 15410−15420.
(11) Bazant, M. Z.; Kilic, M. S.; Storey, B. D.; Ajdari, A. Towards an understanding of induced-charge electrokinetics at large applied voltages in concentrated solutions. *Adv. Colloid Interface Sci.* **2009**, *152*, 48−88.
(12) Kornyshev, A. A. Double-Layer in Ionic Liquids: Paradigm Change? *J. Phys. Chem. B* **2007**, *111*, 5545−5557.
(13) Kilic, M. S.; Bazant, M. Z.; Ajdari, A. Steric effects in the dynamics of electrolytes at large applied voltages. I. Double-layer charging. *Phys. Rev. E* **2007**, *75*, 021502.
(14) Stern, O. Zur theorie der elektrolytischen doppelschicht. *Zeitschrift für Elektrochemie und angewandte physikalische Chemie* **1924**, *30*, 508−516.
(15) Bikerman, J. Structure and capacity of electrical double layer. *London, Edinburgh, and Dublin Philosophical Magazine and Journal of Science* **1942**, *33*, 384−397.
(16) Freise, V. Zur theorie der diffusen doppelschicht. *Zeitschrift für Elektrochemie, Berichte der Bunsengesellschaft für physikalische Chemie* **1952**, *56*, 822−827.
(17) Fedorov, M. V.; Kornyshev, A. A. Towards Understanding the Structure and Capacitance of Electrical Double Layer in Ionic Liquids. *Electrochim. Acta* **2008**, *53*, 6835−6840.
(18) Fedorov, M. V.; Kornyshev, A. A. Ionic liquid near a charged wall: Structure and capacitance of electrical double layer. *J. Phys. Chem. B* **2008**, *112*, 11868−11872.
(19) Lyklema, J. *Solid-Liquid Interfaces*; Fundamentals of Interface and Colloid Science. Volume II; Elsevier, 1995.
(20) Faulkner, L. R.; Bard, A. J. *Electrochemical Methods: Fundamentals and Applications*; John Wiley and Sons, 2002.
(21) Bazant, M. Z.; Storey, B. D.; Kornyshev, A. A. Double Layer in Ionic Liquids: Overscreening versus Crowding. *Phys. Rev. Lett.* **2011**, *109*, 046102.
(22) de Souza, J. P.; Goodwin, Z. A. H.; McEldrew, M.; Kornyshev, A. A.; Bazant, M. Z. Interfacial Layering in the Electric Double Layer of Ionic Liquids. *Phys. Rev. Lett.* **2020**, *125*, 116001.
(23) Goodwin, Z. A. H.; de Souza, J. P.; Bazant, M. Z.; Kornyshev, A. A. In *Encyclopedia of Ionic Liquids*; Zhang, S., Ed.; Springer Singapore: Singapore, 2021; pp 1−13.
(24) Wu, J.; Jiang, T.; Jiang, D.-e.; Jin, Z.; Henderson, D. A classical density functional theory for interfacial layering of ionic liquids. *Soft Matter* **2011**, *7*, 11222−11231.
(25) Jiang, D.-e.; Wu, J. Microscopic insights into the electrochemical behavior of nonaqueous electrolytes in electric double-layer capacitors. *J. Phys. Chem. Lett.* **2013**, *4*, 1260−1267.
(26) McEldrew, M.; Goodwin, Z. A.; Kornyshev, A. A.; Bazant, M. Z. Theory of the double layer in water-in-salt electrolytes. *J. Phys. Chem. Lett.* **2018**, *9*, 5840−5846.
(27) Han, Y.; Huang, S.; Yan, T. A Mean-Field Theory on the Differential Capacitance of Asymmetric Ionic Liquid Electrolytes. *J. Phys.: Condens. Matter* **2014**, *26*, 284103.
(28) Gongadze, E.; Iglič, A. Asymmetric size of ions and orientational ordering of water dipoles in electric double layer model-an analytical mean-field approach. *Electrochim. Acta* **2015**, *178*, 541−545.
(29) Maggs, A. C.; Podgornik, R. General theory of asymmetric steric interactions in electrostatic double layers. *Soft Mater.* **2016**, *12*, 1219−1229.
(30) Popović, M.; Šiber, A. Lattice-gas Poisson-Boltzmann Approach for Sterically Asymmetric Electrolytes. *Phys. Rev. E* **2013**, *88*, 022302.
(31) Yin, L.; Huang, Y.; Chen, H.; Yan, T. A mean-field theory on the differential capacitance of asymmetric ionic liquid electrolytes. II. Accounts of ionic interactions. *Phys. Chem. Chem. Phys.* **2018**, *20*, 17606−17614.
(32) Jiang, D.-e.; Meng, D.; Wu, J. Density functional theory for differential capacitance of planar electric double layers in ionic liquids. *Chem. Phys. Lett.* **2011**, *504*, 153−158.
(33) Henderson, D.; Lamperski, S.; Jin, Z.; Wu, J. Density functional study of the electric double layer formed by a high density electrolyte. *J. Phys. Chem. B* **2011**, *115*, 12911−12914.
(34) Cats, P.; Evans, R.; Härtel, A.; van Roij, R. Primitive model electrolytes in the near and far field: Decay lengths from DFT and simulations. *J. Chem. Phys.* **2021**, *154*, 124504.
(35) Roth, R.; Gillespie, D. Shells of charge: a density functional theory for charged hard spheres. *J. Phys.: Condens. Matter* **2016**, *28*, 244006.
(36) Gillespie, D.; Nonner, W.; Eisenberg, R. S. Density functional theory of charged, hard-sphere fluids. *Phys. Rev. E* **2003**, *68*, 031503.
(37) Härtel, A. Structure of electric double layers in capacitive systems and to what extent (classical) density functional theory describes it. *J. Phys.: Condens. Matter* **2017**, *29*, 423002.
(38) Henderson, D.; Blum, L.; Smith, W. R. Application of the hypernetted chain approximation to the electric double layer at a charged planar interface. *Chem. Phys. Lett.* **1979**, *63*, 381−383.
(39) Carnie, S. L.; Chan, D. Y.; Mitchell, D. J.; Ninham, B. W. The structure of electrolytes at charged surfaces: the primitive model. *J. Chem. Phys.* **1981**, *74*, 1472−1478.
(40) Ennis, J.; Kjellander, R.; Mitchell, D. J. Dressed ion theory for bulk symmetric electrolytes in the restricted primitive model. *J. Chem. Phys.* **1995**, *102*, 975−991.
(41) Attard, P. Asymptotic analysis of primitive model electrolytes and the electrical double layer. *Phys. Rev. E* **1993**, *48*, 3604.
(42) Leote de Carvalho, R.; Evans, R. The decay of correlations in ionic fluids. *Mol. Phys.* **1994**, *83*, 619−654.
(43) Guerrero-García, G. I.; González-Tovar, E.; Lozada-Cassou, M.; de J. Guevara-Rodríguez, F. The electrical double layer for a fully asymmetric electrolyte around a spherical colloid: An integral equation study. *J. Chem. Phys.* **2005**, *123*, 034703.
(44) Greberg, H.; Kjellander, R. Charge inversion in electric double layers and effects of different sizes for counterions and coions. *J. Chem. Phys.* **1998**, *108*, 2940−2953.
(45) Israelachvili, J. N. *Intermolecular and Surface Forces*; Academic Press, 2015.
(46) Ueno, K.; Kasuya, M.; Watanabe, M.; Mizukami, M.; Kurihara, K. Resonance shear measurement of nanoconfined ionic liquids. *Phys. Chem. Chem. Phys.* **2010**, *12*, 4066−4071.
(47) Hayes, R.; Borisenko, N.; Tam, M. K.; Howlett, P. C.; Endres, F.; Atkin, R. Double layer structure of ionic liquids at the Au (111) electrode interface: an atomic force microscopy investigation. *J. Phys. Chem. C* **2011**, *115*, 6855−6863.
(48) Smith, A. M.; Perkin, S.; et al. Switching the structural force in ionic liquid-solvent mixtures by varying composition. *Phys. Rev. Lett.* **2017**, *118*, 096002.

https://doi.org/10.1021/acs.jpcb.1c09441
J. Phys. Chem. B 2022, 126, 1242−1253

(49) Lee, A. A.; Perez-Martinez, C.; Smith, A. M.; Perkin, S. Underscreening in concentrated electrolytes. *Faraday Discuss.* **2017**, *199*, 239.
(50) Gebbie, M. A.; Smith, A. M.; Dobbs, H. A.; Lee, A. A.; Warr, G. G.; Banquy, X.; Valtiner, M.; Rutland, M. W.; Israelachvili, J. N.; Perkin, S.; Atkin, R. Long range electrostatic forces in ionic liquids. *Chem. Commun.* **2017**, *53*, 1214−1224.
(51) Smith, A. M.; Lee, A. A.; Perkin, S. The Electrostatic Screening Length in Concentrated Electrolytes Increases with Concentration. *J. Phys. Chem. Lett.* **2016**, *7*, 2157−2163.
(52) Fajardo, O.; Bresme, F.; Kornyshev, A.; Urbakh, M. Electrotunable lubricity with ionic liquid nanoscale films. *Sci. Rep.* **2015**, *5*, 1−7.
(53) Fajardo, O. Y.; Bresme, F.; Kornyshev, A. A.; Urbakh, M. Electrotunable friction with ionic liquid lubricants: how important is the molecular structure of the ions? *J. Phys. Chem. Lett.* **2015**, *6*, 3998−4004.
(54) Merlet, C.; Péan, C.; Rotenberg, B.; Madden, P. A.; Simon, P.; Salanne, M. Simulating supercapacitors: Can we model electrodes as constant charge surfaces? *J. Phys. Chem. Lett.* **2013**, *4*, 264−268.
(55) Haskins, J. B.; Lawson, J. W. Evaluation of molecular dynamics simulation methods for ionic liquid electric double layers. *J. Chem. Phys.* **2016**, *144*, 184707.
(56) Ntim, S.; Sulpizi, M. Role of image charges in ionic liquid confined between metallic interfaces. *Phys. Chem. Chem. Phys.* **2020**, *22*, 10786−10791.
(57) Kondrat, S.; Georgi, N.; Fedorov, M. V.; Kornyshev, A. A. A superionic state in nano-porous double-layer capacitors: insights from Monte Carlo simulations. *Phys. Chem. Chem. Phys.* **2011**, *13*, 11359−11366.
(58) Di Lecce, S.; Kornyshev, A. A.; Urbakh, M.; Bresme, F. Structural effects in nanotribology of nanoscale films of ionic liquids confined between metallic surfaces. *Phys. Chem. Chem. Phys.* **2021**, *23*, 22174−22183.
(59) Giera, B.; Henson, N.; Kober, E. M.; Shell, M. S.; Squires, T. M. Electric double-layer structure in primitive model electrolytes: comparing molecular dynamics with local-density approximations. *Langmuir* **2015**, *31*, 3553−3562.
(60) Valleau, J. P.; Cohen, L. K. Primitive model electrolytes. I. Grand canonical Monte Carlo computations. *J. Chem. Phys.* **1980**, *72*, 5935−5941.
(61) Valiskó, M.; Kristóf, T.; Gillespie, D.; Boda, D. A systematic Monte Carlo simulation study of the primitive model planar electrical double layer over an extended range of concentrations, electrode charges, cation diameters and valences. *AIP Advances* **2018**, *8*, 025320.
(62) Jiang, J.; Cao, D.; Henderson, D.; Wu, J. Revisiting density functionals for the primitive model of electric double layers. *J. Chem. Phys.* **2014**, *140*, 044714.
(63) Frydel, D.; Levin, Y. The double-layer of penetrable ions: An alternative route to charge reversal. *J. Chem. Phys.* **2013**, *138*, 174901.
(64) Frydel, D. The double-layer structure of overscreened surfaces by smeared-out ions. *J. Chem. Phys.* **2016**, *145*, 184703.
(65) Roth, R. Fundamental measure theory for hard-sphere mixtures: a review. *J. Phys.: Condens. Matter* **2010**, *22*, 063102.
(66) Carnahan, N. F.; Starling, K. E. Equation of state for nonattracting rigid spheres. *J. Chem. Phys.* **1969**, *51*, 635−636.
(67) Andelman, D. Introduction to electrostatics in soft and biological matter. *Soft condensed matter physics in molecular and cell biology* **2006**, *6*, 97.
(68) Ravikovitch, P. I.; Neimark, A. V. Density functional theory model of adsorption deformation. *Langmuir* **2006**, *22*, 10864−10868.
(69) Ravikovitch, P. I.; Neimark, A. V. Density functional theory model of adsorption on amorphous and microporous silica materials. *Langmuir* **2006**, *22*, 11171−11179.
(70) Henderson, J. Statistical mechanics of the disjoining pressure of a planar film. *Phys. Rev. E* **2005**, *72*, 051602.

https://doi.org/10.1021/acs.jpcb.1c09441
J. Phys. Chem. B 2022, 126, 1242−1253